

Adipose-derived Stem/Stromal Cells on Electrospun Fibrin Microfiber Bundles Enable Moderate Muscle Reconstruction in a Volumetric Muscle Loss Model

Jordana Gilbert-Honick^{1,2}, Brian Ginn^{1,3,4}, Yuanfan Zhang^{5,6}, Sara Salehi¹, Kathryn R. Wagner^{5,6,7}, Hai-Quan Mao^{1,2,3,4}, and Warren L. Grayson^{1,2,3,4} 

Cell Transplantation
2018, Vol. 27(11) 1644–1656
© The Author(s) 2018
Article reuse guidelines:
sagepub.com/journals-permissions
DOI: 10.1177/0963689718805370
journals.sagepub.com/home/cll


Abstract

Current treatment options for volumetric muscle loss (VML) are limited due to donor site morbidity, lack of donor tissue, and insufficient functional recovery. Tissue-engineered skeletal muscle grafts offer the potential to significantly improve functional outcomes. In this study, we assessed the potential pro-myogenic effects of human adipose-derived stem cells (ASCs) seeded onto electrospun uniaxially aligned fibrin hydrogel microfiber bundles. Although both uninduced and 5-azacytidine-induced ASCs exhibited alignment, elongation, and diffuse muscle marker expression when grown on microfiber bundles for 2 months *in vitro*, both groups failed to fully recapitulate myotube characteristics. To assess the muscle regeneration potential of ASCs *in vivo*, ASC-seeded fibrin microfiber bundles were implanted in a robust murine VML defect model. Minimal fibrosis was observed surrounding implanted acellular hydrogel fibers at 2 and 4 weeks, and fibers seeded with ASCs exhibited up to 4 times higher volume retention than acellular fibers. We observed increased numbers of cells positive for the regenerating muscle marker embryonic myosin and the mature muscle marker myosin heavy chain in ASC-seeded fibers compared with acellular fibers at 1 and 3 months post-transplantation. Regenerating muscle cells were closely associated with ASC-derived cells and in some cases had potentially fused with them. These findings demonstrate that despite failing to undergo myogenesis *in vitro*, ASCs combined with electrospun fibrin microfibrils moderately increased muscle reconstruction *in vivo* compared with acellular fibers following a severe VML defect.

Keywords

skeletal muscle, tissue engineering, adipose-derived stem cell, electrospinning, fibrin, volumetric muscle loss

¹ Translational Tissue Engineering Center, Johns Hopkins University School of Medicine, Baltimore, MD, USA

² Department of Biomedical Engineering, Johns Hopkins University School of Medicine, Baltimore, MD, USA

³ Department of Materials Science and Engineering, Johns Hopkins University, Baltimore, MD, USA

⁴ Institute for NanoBioTechnology, Johns Hopkins University, Baltimore, MD, USA

⁵ The Hugo W. Moser Research Institute, Kennedy Krieger Institute, Baltimore, MD, USA

⁶ Graduate Program in Cellular and Molecular Medicine, Johns Hopkins School of Medicine, Baltimore, MD, USA

⁷ Departments of Neurology and Neuroscience, Johns Hopkins School of Medicine, Baltimore, MD, USA

Submitted: May 23, 2018. Revised: August 22, 2018. Accepted: September 12, 2018.

Corresponding Author:

Warren L. Grayson, Translational Tissue Engineering Center, Johns Hopkins University School of Medicine, 400 N. Broadway, Smith Building 5023, Baltimore, MD 21231, USA.

Email: wgrayson@jhmi.edu



Creative Commons Non Commercial CC BY-NC: This article is distributed under the terms of the Creative Commons Attribution-NonCommercial 4.0 License (<http://www.creativecommons.org/licenses/by-nc/4.0/>) which permits non-commercial use, reproduction and distribution of the work without further permission provided the original work is attributed as specified on the SAGE and Open Access pages (<https://us.sagepub.com/en-us/nam/open-access-at-sage>).

Introduction

Volumetric muscle loss (VML) occurs when a tissue defect exceeds 20% of an individual muscle volume, which overwhelms the natural repair mechanism and leads to chronic functional deficits in the affected muscle¹. Limited treatment options for VML include transfer of an autologous free muscle flap², muscle transposition¹, amputation, and power bracing². These treatments have low success rates in restoring muscle function, and at best provide aesthetic benefits and prevent further necrosis^{1,2}. They are also limited by donor site morbidity, lack of donor tissue, and the need for a highly skilled surgical team, which complicate VML treatment and lead to unsatisfactory patient outcomes². Tissue-engineered (TE) grafts offer a potentially more effective regenerative medicine treatment option for VML that may alleviate the varied limitations of current treatments and lead to improved functional outcomes.

A range of materials have been utilized as scaffolds to treat VML with varied results, including decellularized extracellular matrix (ECM)^{3–10}, collagen¹¹, hyaluronic acid¹², fibrin^{13–15}, keratin^{16,17}, gelatin^{18,19}, and poly(lactic acid)/poly(lactic-co-glycolic acid) (PLA/PLGA)²⁰. Our group has demonstrated the capacity to enhance the bioactivity and biocompatibility of fibrin by electrospinning it into microfiber bundles with alignment topography, tunable substrate stiffness, and controllable porous architecture²¹. Alignment cues have been shown to strongly enhance stem cell myogenic differentiation as well as myocyte fusion^{22,23}. Electrospun hydrogels can be tuned to physiological stiffness to enhance myogenesis, as substrate stiffness has been reported to strongly affect stem cell differentiation and myogenesis^{24,25}. We have recently successfully treated a murine VML defect consisting of partial resection of the tibialis anterior muscle by combining the electrospun fibrin microfiber bundles and C2C12 myoblasts²⁶.

Adipose-derived stem/stromal cells (ASCs) are clinically translatable, and previous studies have shown them to be a promising cell source for applications in skeletal muscle regeneration^{27–31}. While a number of groups have researched myoblasts³², satellite cells¹², or mesangioblasts³³ for skeletal muscle tissue engineering, the practicality of using these cell types for clinical treatments is limited by their low accessibility, low yield, and difficulty in long-term culture and expansion¹². In contrast, ASCs are isolated from lipoaspirate involving a more mild procedure, and lipoaspirate has 100 times higher stem cell yields than bone marrow, another mesenchymal stem cell source with myogenic potential³⁴. ASCs also have high stem cell proliferation rates²⁷, can differentiate down the myogenic pathway^{27–29}, provide a pro-regenerative environment³⁵, and evade the host immune system³⁶. Although many studies have assessed *in vitro* ASC myogenic potential^{27–29,31,34,37–43}, there have been few studies assessing *in vivo* muscle regeneration using ASCs. It has been shown that ASCs injected into the muscles of dystrophic mice could differentiate into

dystrophin+ mature muscle cells²⁸ with a pool of replenished Pax7+ satellite cells³¹, ASCs seeded onto PLGA microsphere carriers transplanted subcutaneously in nude mice formed new muscle tissue after 60 days⁴⁰, and NG2+ ASCs seeded onto hyaluronic acid scaffolds transplanted subcutaneously in nude mice expressed muscle markers after 30 days⁴⁴. Another study assessed the regenerative potential of rat ASCs in collagen within a murine VML defect and did not see muscle regeneration, although implanting adipose-derived microvascular fragments did result in low levels of muscle regeneration⁴⁵. The ability of rat ASCs in a decellularized extracellular matrix (ECM) to regenerate a murine VML defect was also assessed and resulted in low levels of ASC contribution to regenerating myofibers⁴⁶.

Here, we utilized axially aligned fibrin hydrogel microfiber bundles with an elastic modulus similar to that of native muscle tissues to evaluate the growth and myogenic differentiation of human ASCs seeded on electrospun fibrin microfiber bundles *in vitro* in the absence or presence of biochemical induction cues. Moreover, we assessed the ability of the microfiber bundles with and without ASCs to treat a robust murine VML model, in which the entire tibialis anterior (TA) and extensor digitorum longus (EDL) muscles were both removed. We tested the hypothesis that the combination of human ASCs on electrospun fibrin fibers promotes muscle regeneration and that *ex vivo* differentiation of ASCs down a myogenic lineage prior to transplantation would significantly enhance this response.

Materials and Methods

Electrospinning Fibrin Fiber Bundles

Fibrin fibers were electrospun in a sterile environment with sterile solutions using a protocol that has been described previously^{21,26}. Briefly, parallel syringes containing sterile solutions of fibrinogen (Sigma-Aldrich, St. Louis, MO, USA) or sodium alginate (Sigma-Aldrich) were connected via a y-syringe and extruded by syringe pumps with an applied voltage of 3–5 kV applied to a blunted 27G needle tip to form hydrogel microfiber bundles. Polyethylene oxide (average MW ~ 4,000 kDa, Sigma-Aldrich) was added to each solution at 0.2 wt% to increase viscosity during electrospinning. The electrospun hydrogel solutions were collected for 5.75 minutes on a rotating dish (~35 rpm) containing 50 mM CaCl₂ and 20 U/ml thrombin (Sigma-Aldrich) as crosslinking agents. Samples were crosslinked an additional 3–5 min after electrospinning and were then wrapped around a 1.5 × 3.0 cm mylar frame 3–4 times to yield a hydrogel fiber bundle ~1 mm in diameter. Fibers were incubated overnight in 250 mM sodium citrate (Sigma-Aldrich) to dissolve the alginate and then transferred to deionized (DI) water until cell seeding or implantation. The resulting fibers have a tensile modulus of 17 kPa, and are saturable and remain elastic when strained up to 50% of their length.

Cell Culture

ASCs were isolated from lipoaspirate tissue under an institutional review board-approved protocol as previously described⁴⁷. Two female donor sources were used: a 39-year-old Caucasian and a 63-year-old African American. *In vitro* studies utilized ASCs from both donors while *in vivo* studies utilized ASCs from the first donor. Briefly, tissue was digested with collagenase (1 mg/mL; Worthington Biochemical Corp., Lakewood, NJ, USA) to isolate the stromal vascular fraction of cells. These cells were plated onto tissue culture plastic and were termed "passage 0 ASC" when they reached 80–90% confluence. These cells were cryopreserved for future studies. ASCs were thawed and expanded for two passages in Growth Medium: high-glucose DMEM (ThermoFisher Scientific, Waltham, MA, USA) with 10% fetal bovine serum (FBS; Atlanta Biologicals, Flowery Branch, GA, USA), 1% penicillin/streptomycin (P/S; ThermoFisher Scientific), and 1 ng/mL FGF-2 (PeproTech, Rocky Hill, NJ, USA). The ASCs were then trypsinized and used at passage 3 for all experiments. The phenotypic profile of the cells at this passage from both donors was examined via flow cytometry for mesenchymal (CD73, CD90, CD105) and vascular markers (CD31, CD34). Briefly, ASCs at passage 1 were thawed and expanded as described above. Passage 3 ASCs were then suspended in phosphate-buffered saline (PBS) containing 2% FBS and incubated with monoclonal antibodies conjugated to fluorescein isothiocyanate or phycoerythrin for 30 min at 4°C. Cells were then analyzed with a flow cytometer (BD Accuri C6, BD Biosciences, San Jose, CA, USA). All antibodies were purchased from BD Biosciences.

Cell Seeding and Growth on Fibers

Fibers fabricated with 15% alginate were utilized for all experiments. In preparation for cell seeding, fibers were incubated in high-glucose DMEM for 20 min at 37°C. The fibers were then transferred to cell culture plates coated with 2% agarose type VII (Sigma-Aldrich) to minimize cell adhesion to the plate surface and increase seeding efficiency onto the fibers. For the seeding density study a seeding volume of 15 μ l at either 10,000, 20,000, or 40,000 cells/ μ l was pipetted onto the fiber surface. All subsequent *in vitro* and *in vivo* studies used 15 μ l at 40,000 cell/ μ l (for a total seeding density of 600,000 cells/fiber bundle). Fibers with cells were incubated for 1 hour at 37°C with hydration levels maintained by addition of 15 μ l of Growth Medium halfway through. After the 1-hour incubation, Control Medium (high-glucose DMEM, 10% FBS, 1% P/S, 30 μ g/ml aprotinin (ThermoFisher Scientific), and 1 ng/mL FGF-2) was added to fully submerge the fibers. Media was changed 24 hours post-seeding and then every other day until harvest.

Myogenic Induction

Induction of ASCs toward myogenesis was performed with an adapted protocol previously described⁴⁸. After 7 days of growth in Control Medium fibers were transferred to Induction Medium: low glucose DMEM (ThermoFisher Scientific) with 1% FBS, 5% horse serum (HS; ThermoFisher Scientific), 1% P/S, 30 μ g/ml aprotinin, and 10 μ M 5-azacytidine (Aza; Sigma-Aldrich). After 24 hours the fibers were rinsed with PBS and returned to Control Medium for the duration of the experiment.

Cell Viability

To compare cell viability and morphology a Live/Dead Viability/Cytotoxicity Kit (ThermoFisher Scientific) was used at a range of seeding densities. Samples were incubated with calcein AM and ethidium homodimer-1 for 20 min then imaged with a confocal microscope (Zeiss LSM 510, Oberkochen, Germany).

PicoGreen Assays

DNA content of seeded cells on the fibers at various densities was quantified using a PicoGreen dsDNA quantitation kit (ThermoFisher Scientific). Cells were lysed by placing whole fibers in 500 μ l of digestion buffer (10 mM Tris, 1 mM EDTA, 0.1% Triton X-100, and 0.1 mg/mL proteinase K) before incubation with PicoGreen and reading with a fluorescent plate reader (BioTek, Winooski, VT, USA) at excitation 485 nm and emission 530 nm. Cellular infiltration into the fiber interior was assessed using 10 μ m-thick cryosections and staining for 30 min with DAPI (Sigma-Aldrich).

Whole Mount Immunostaining

Samples were fixed in ice-cold methanol at –20°C overnight then rinsed three times for 20 min each. Fibers were then cut from their frames and placed in 0.5 ml tubes for subsequent staining steps. Fibers were blocked and permeabilized (Block/Perm) for 3 hours with 0.2% Triton X-100 and 5% normal goat serum (Sigma-Aldrich) in PBS with 0.1% Tween (PTw). Fibers were then incubated with primary antibodies diluted in blocking solution overnight at 4°C on a rocker at 135 rpm followed by three 1-hour washes with PTw. Primary antibodies included mouse anti-myogenin (5 μ g/ml; DSHB, Iowa City, IA, USA) and rabbit anti-desmin (2.7 μ g/ml; Santa Cruz Biotechnology, Dallas, TX, USA). Fibers were then incubated with DyLight 488-conjugated goat anti-mouse and DyLight 649-conjugated goat anti-rabbit (both 1:400; Jackson ImmunoResearch, West Grove, PA, USA) diluted in blocking solution overnight at 4°C on a rocker at 135 rpm, followed by three 1 hour washes with PTw. DAPI was incorporated in the second wash at a dilution of 1:2,000. Samples were then imaged with a confocal microscope.

To visualize cell morphology and multinucleation, fibers were fixed with 3.7% formaldehyde at 4°C for 3 hours and then washed with PBS three times for 20 min each. Fibers were then cut from their frames and incubated in Block/Perm for 3 hours at 4°C. A staining solution containing Phalloidin-TRITC (12.5 µg/ml; Sigma-Aldrich) and DAPI (1:2,000) was diluted in 0.1% PTw and incubated with fibers for 1 hour at room temperature on a slow rocker. Fibers were washed three times for 20 min each in 0.1% PTw then imaged with a confocal microscope.

VML Defect Model

Animal and surgical procedures were approved by the Institutional Animal Care and Use Committee at Johns Hopkins University School of Medicine. For the acellular scaffold study 10 two-month-old male NOD-Rag1^{null} IL2Rg^{null} (NRG) immunodeficient mice (Jackson Lab, Bar Harbor, ME, USA) were used and for the cell-seeded scaffold study 14 two-month-old female NOD-scid IL2Rg^{null} (NSG) immunodeficient mice (Jackson Lab) were used (Supplemental Fig. 2). Two strains of immunodeficient mice were utilized due to availability of mice at the time of the study. NRG and NSG mice are phenotypically very similar and both are highly immunodeficient with the only known phenotypic difference related to radiation/chemotherapy sensitivity, which was not relevant to this study. Mice were anesthetized with isoflurane and the TA and EDL muscles were removed from the anterior tibial compartment in a bilateral defect on all mice, as described previously⁴⁹. Care was taken to ensure bleeding had ceased before 1 or 3 fiber bundles were placed in the empty defect site and ligated on both ends to the tendons of the peroneus longus muscle with non-absorbable sutures (6/0 POLYPRO, CP Medical, Norcross, GA, USA) (as shown in Fig. 2A). Surgical glue (Histoacryl, B. Braun Medical, Bethlehem, PA, USA) and stainless steel wound clips (Reflex Wound Clips, CellPoint Scientific, Gaithersburg, MD, USA) were used to close the skin. Rimadyl (Patterson Veterinary, Greeley, CO, USA) was given at 5 mg/kg subcutaneously post-surgery for pain management. For the cell-seeded study, acellular fibers were incubated for 24 hours in Control Medium before implantation. Upon harvest, fibers were removed along with the surrounding native muscle tissue. One mouse containing acellular and uninduced fibers died before the 3-month study ended and was excluded from data analysis.

Histology

Mice were sacrificed at 2, 4, and 12 weeks, and the portion of their hind-limb containing the scaffold and surrounding muscle tissue was harvested and frozen in optimal cutting temperature (OCT) compound. Samples were cut into 10 µm sections on a cryostat, dried on Superfrost Plus slides, and rehydrated in DI water before staining with Masson's Trichrome (Sigma-Aldrich) stain. Slides were imaged on an

Axio Imager upright microscope (Zeiss). Fibrosis was quantified with Image J software (NIH, Rockville, MD, USA) by measuring the collagen area and fiber cross-sectional area ($n=15$: 5 samples with 3 cryosections per sample). In both the acellular and cell-seeded *in vivo* studies, fibrosis was normalized to the cross-sectional area of the implanted fibrin fiber for each sample. In the cell-seeded *in vivo* experiment, relative cross-sectional area was determined by comparing the cross-sectional areas of cell-seeded samples with the average cross-sectional area of 2-week acellular controls (containing 3 fibers/defect).

Immunohistochemistry

Samples were cryosectioned as described above. Slides were fixed in ice-cold methanol for 10 min, rinsed with PBS three times for 15 min each, and then blocked in 10% normal donkey serum (Sigma-Aldrich) in PBS for 1 hour at RT. For CD31 staining, slides were fixed in ice-cold acetone for 10 min, rinsed with PBS, then blocked in 10% normal goat serum (Sigma-Aldrich). Slides were incubated with antigen-specific primary antibodies in blocking solution overnight at 4°C. Primary antibodies included rabbit anti-mouse CCR7 (2.6 µg/ml; Abcam, Cambridge, UK), rabbit anti-human LaminAC (1.1 µg/ml; Abcam), mouse anti-human LaminAC (1:20; Abcam), mouse anti-embryonic myosin (4 µg/ml; DSHB), mouse anti-myosin heavy chain (24.3 µg/ml; Sigma-Aldrich), rabbit anti-laminin (4.5 µg/ml; Sigma-Aldrich), and rat anti-mouse CD31 (0.3 µg/ml; BD Biosciences). The embryonic myosin (eMHC), myosin heavy chain (MHC), and laminin antibodies have reactivity for both mouse and human proteins. After three 15 min washes with PBS, slides were incubated with Cy3-conjugated donkey anti-mouse, Alexa Fluor 647-conjugated donkey anti-rabbit (both 1:400; Jackson ImmunoResearch), or Alexa Fluor 594-conjugated goat anti-rat (1:500; ThermoFisher Scientific) and DAPI (1:1,000) diluted in blocking solution for 1 hour at room temperature. Slides were washed three times for 15 min then mounted with 50% glycerol and imaged on an Axio Observer inverted fluorescence microscope (Zeiss). To quantify immunostaining, CCR7 area was measured with ImageJ and cells staining positive for eMHC and MHC were counted manually.

Statistics

Statistical analysis was performed using GraphPad Prism 5 software (GraphPad Software, La Jolla, CA, USA). Statistical significance for the DNA assay was determined by one-way analysis of variance (ANOVA) with Tukey's post-test ($n=3$). In the first *in vivo* study assessing acellular scaffolds, statistical significance for fibrosis and CCR7 areas ($n=14-16$) was determined by unpaired two-tailed *t*-test. For the second *in vivo* study assessing cell-seeded scaffolds, statistical significance for fibrosis areas and immunostained samples ($n=9-15$) was determined with one-way ANOVA with

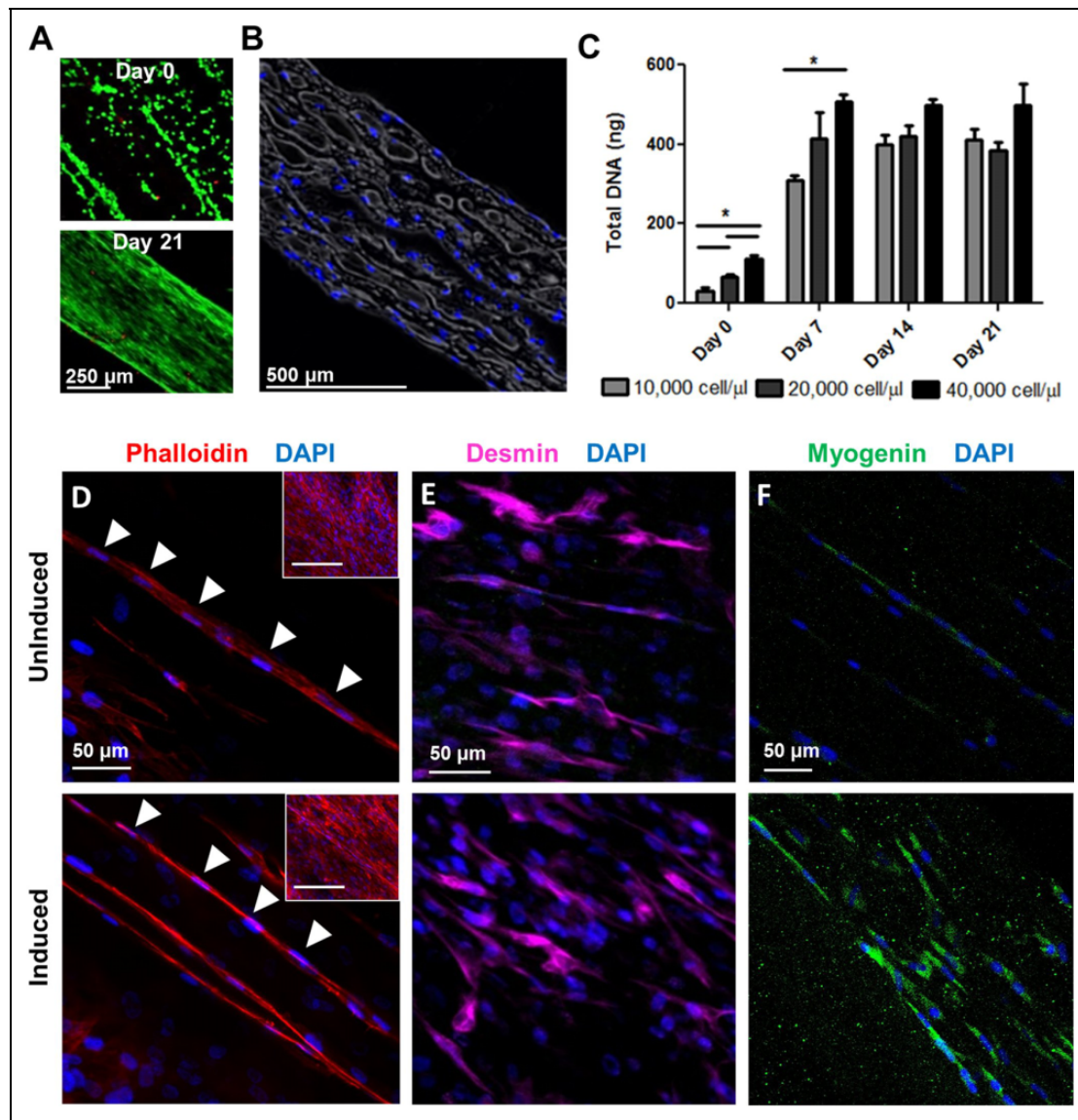


Fig 1. ASC growth and myogenesis on electrospun fibrin fibers. (A) Live (green)/Dead (red) staining of cells seeded at 40 000 cells/ μ l at days 0 and 21. (B) Histological cross-section stained with DAPI (blue) showing ASC infiltration to the fiber interior at day 21. (C) Quantification of total DNA content of fibers seeded with ASCs at the three seeding densities at days 0, 7, 14, and 21. * $p < 0.05$ (D) Phalloidin (red) and DAPI (blue) staining illustrating some multinucleation of ASCs on fibers at 2 months in both uninduced and induced groups. Arrows demonstrate aligned and elongated nuclei within potential myotubes. Inset: lower magnification image of phalloidin staining. Scale bar: 200 μ m. (E) Desmin (purple) and (F) myogenin (green) staining ASCs grown on fibers in both uninduced and induced groups at 2 months.

Dunnet post-test. Statistical significance when assessing percent of ASCs in the defect ($n=12-15$) was assessed with an unpaired two-tailed t -test.

Results

ASCs Align on Fiber Surface and Infiltrate into the Interior of Fiber Bundle

ASCs at passage 3 from both donors highly expressed the mesenchymal markers CD73, CD90, and CD105 and had negligible to very low expression of the vascular markers

CD31, CD34 (Supplemental Table 1, Supplemental Fig. 1). ASCs were seeded onto the fibers and proliferated to cover the fiber surfaces, aligning with the major axis of the fibers with good cell viability at a range of seeding densities and time points (Fig. 1A). There were no visible differences in cell morphology at the three seeding densities from days 7–21. ASCs became confluent on the fiber surface by day 7 and maintained their confluency through day 21. In addition to covering the fiber surface, ASCs also migrated into the porous fiber interior (Fig. 1B). DNA quantification was used to assess cell numbers at different times in culture. Differences

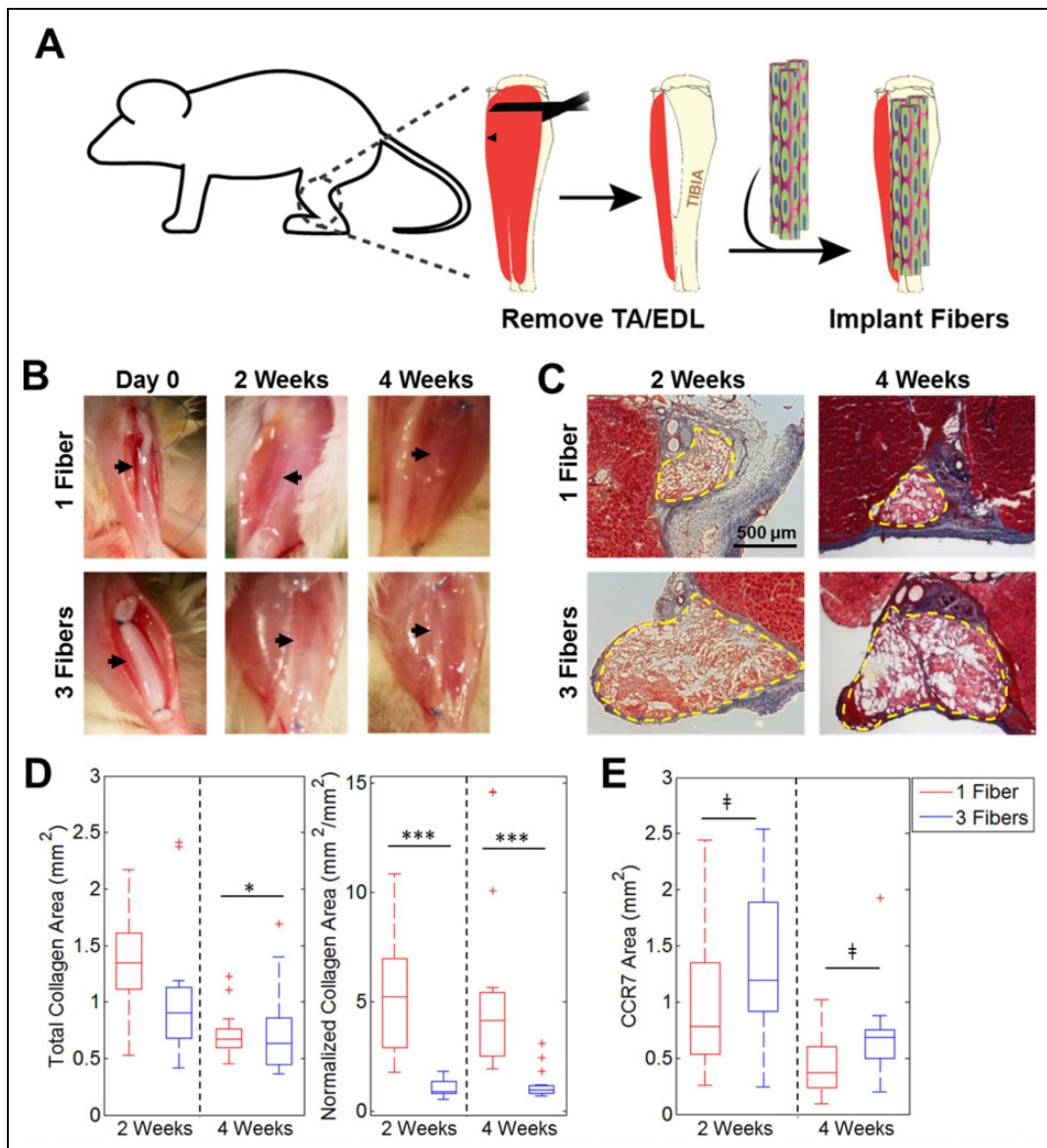


Fig 2. Fibrosis resulting from implantation of acellular fibers into VML defect. (A) Schematic illustrating fiber implantation into a murine VML defect model. (B) Gross images of defects with 1 or 3 fibers/defect at Day 0 and 2 or 4 weeks post-transplantation. Black arrows illustrate fiber location within defect site. (C) Masson's Trichrome staining demonstrates varying levels of fibrosis among groups. Dashed yellow lines denote fiber boundaries. (D) Quantification of total collagen area and normalized collagen area over time for both groups ($n=14-15$). (E) Quantification of total CCR7 staining area ($n=15$).

* $p < 0.05$. *** $p < 0.001$, †not significant.

in DNA content were statistically significant among the three seeding densities at day 0 and day 7 but not later time points (Fig. 1C). The maximum total DNA content was statistically similar among all groups on days 14 and 21. A seeding density of 40,000 cell/ μl was selected for subsequent studies because of its higher DNA content at earlier time points.

ASCs Do Not Fully Replicate Myotube Characteristics at Two Months In Vitro

After 2 months of *in vitro* culture, phalloidin staining of both uninduced and induced ASCs on the fibers revealed the

presence of long tubes of cells in the fiber interior with elongated and aligned nuclei that paralleled the fiber's major axis and mimicked the appearance of multinucleated myotubes (Fig. 1D). Although both uninduced and induced groups expressed high levels of desmin, a muscle structural protein (Fig. 1E), expression of the muscle transcription factor myogenin was low and non-nuclear (Fig. 1F). Interestingly, although ASCs cultured for 2 months did not replicate myotube multinucleation and protein expression completely, there were no significant differences between uninduced and induced samples. This indicates that 5-azacytidine did not provoke a significant pro-myogenic benefit and suggests that

the fiber alignment and stiffness alone may encourage ASCs to begin mimicking myotube characteristics.

Fiber Number Determines Fibrotic Response In Vivo

When acellular fibers were implanted, native tissue surrounding the defect sites had a healthy appearance upon removal at 2 and 4 weeks with no visible scarring for both 1 and 3 fibers/defect (Fig. 2B). There was less fibrosis at both time points when 3 fibers/defect were implanted than there was for 1 fiber/defect, as evident by collagen staining with Masson's Trichrome stain (Fig. 2C). When quantifying total collagen area per sample, the mean values at 2 weeks were 1.36 mm² for 1 fiber/defect and 1.05 mm² for 3 fibers/defect, and at 4 weeks were 0.72 mm² for 1 fiber/defect and 0.73 mm² for 3 fibers/defect. Only the two 4-week groups had a significant difference with 1 fiber yielding significantly more collagen than 3 fibers, although fibrosis in both groups did decrease over time (Fig. 2D). There were significant differences in normalized fibrosis (fibrotic area (mm²)/scaffold cross-sectional area (mm²)) between 1 fiber and 3 fibers at both time points. When quantifying normalized fibrosis, the mean values at 2 weeks were 5.28 (mm²/mm²) for 1 fiber/defect and 0.99 mm²/mm² for 3 fibers/defect, and at 4 weeks were 5.43 mm²/mm² for 1 fiber/defect and 1.19 mm²/mm² for 3 fibers/defect. Differences between normalized fibrosis levels for 1 fiber/defect and 3 fibers/defect were statistically significant at both 2 and 4 weeks. Samples were stained with the M1 macrophage marker CCR7 and areas stained within the fibers were quantified. There were no statistically significant differences in macrophage content between groups at both time points (Fig. 2E).

Cell-Seeded Scaffolds Retain Fiber Cross-Sectional Area

Bilateral murine VML defects were implanted with three fibers/defect that were acellular, uninduced, or induced and harvested after 1 or 3 months. The schematic in Fig. 3A demonstrates how fibers were distributed in the 14 mice used for this study. Upon removal at 1 month, there were distinct visible differences in the appearances of cell-seeded versus acellular fibers, where both cell-seeded groups had robust, opaque fibers visible between the sutures while the acellular fibers were translucent (Fig. 3B, top). These differences correlated with histology data and Masson's Trichrome staining, where cell-seeded fibers had larger cross-sectional areas than those of acellular fibers (Fig. 3B, bottom). Masson's Trichrome staining also demonstrated that all three groups had minimal fibrosis at both time points and there was no significant difference in normalized fibrosis between all three groups (Fig. 3C). When compared with the cross-sectional area of an early-stage implant, cell-seeded fibers had significantly higher retention of fiber cross-sectional area than acellular fibers at both time points (Fig.

3D). The percentage of ASCs in the cell-seeded fibers was measured comparing the number of human-specific LaminAC+ nuclei with the number of other nuclei in the fiber cross-sections. Over 50% of cells in the fibers were ASCs for both groups at both time points and there were no statistically significant differences in the numbers of ASCs between groups (Fig. 3E).

Limited Expression of Myogenic Markers In Vivo

Immunostaining with eMHC was used to assess the presence of regenerating muscle within the defect site. A small number of eMHC+ cells were visible within the fiber interior in both ASC groups as well as LaminAC+ nuclei distributed throughout the fibers (Fig. 4A). In a few cases there were eMHC+ cells whose nuclei were LaminAC+, indicating that those ASCs had differentiated to myogenic cells or had fused with a native regenerating muscle fiber (Fig. 4A, right). MHC, a mature muscle marker, was found at low levels within the fiber interiors as well (Fig. 4B). Both induced and uninduced samples contained laminin+ cells with human nuclei, further suggesting that some implanted ASCs had fused with or differentiated into regenerating myofibers within the defect (Fig. 4C, Supplemental Fig. 3). At 1 month, there were significantly more eMHC+ cells in fibers with uninduced ASCs than there were in acellular fibers, although there was no significant difference for fibers with induced ASCs. At 3 months, all three groups had similar numbers of eMHC+ cells (Fig. 4D). At 1 month, 67.7 ± 27.0% of eMHC+ cells in fibers with uninduced ASCs and 42.4 ± 34.2% of eMHC+ cells in fibers with induced ASCs had a LaminAC+ nucleus immediately adjacent. At 3 months, 43.0 ± 23.0% of eMHC+ cells in fibers with uninduced ASCs and 49.2 ± 28.8% of eMHC+ cells in fibers with induced ASCs had a LaminAC+ nucleus immediately adjacent. At both 1-month and 3-month time points, there were significantly more MHC+ cells in fibers with uninduced ASCs than there were in acellular fibers. Fibers with induced ASCs, however, had similar numbers of MHC+ cells to those in acellular fibers at both time points. At 1 month, 41.8 ± 32.6% of MHC+ cells in fibers with uninduced ASCs and 27.5 ± 28.2% of MHC+ cells in fibers with induced ASCs had a LaminAC+ nucleus immediately adjacent. At 3 months, 61.6 ± 33.0% of MHC+ cells in fibers with uninduced ASCs and 43.8 ± 35.6% of MHC+ cells in fibers with induced ASCs had a LaminAC+ nucleus immediately adjacent. When cross-sections of the excised defect site at 12 weeks were stained for mouse CD31, host vascular infiltration was apparent within the fibers among all three groups (Fig. 4E).

Discussion

There are limited therapeutic options available for the treatment of VML. ASCs are potentially advantageous for TE muscle because of their ease of isolation, higher stem cell

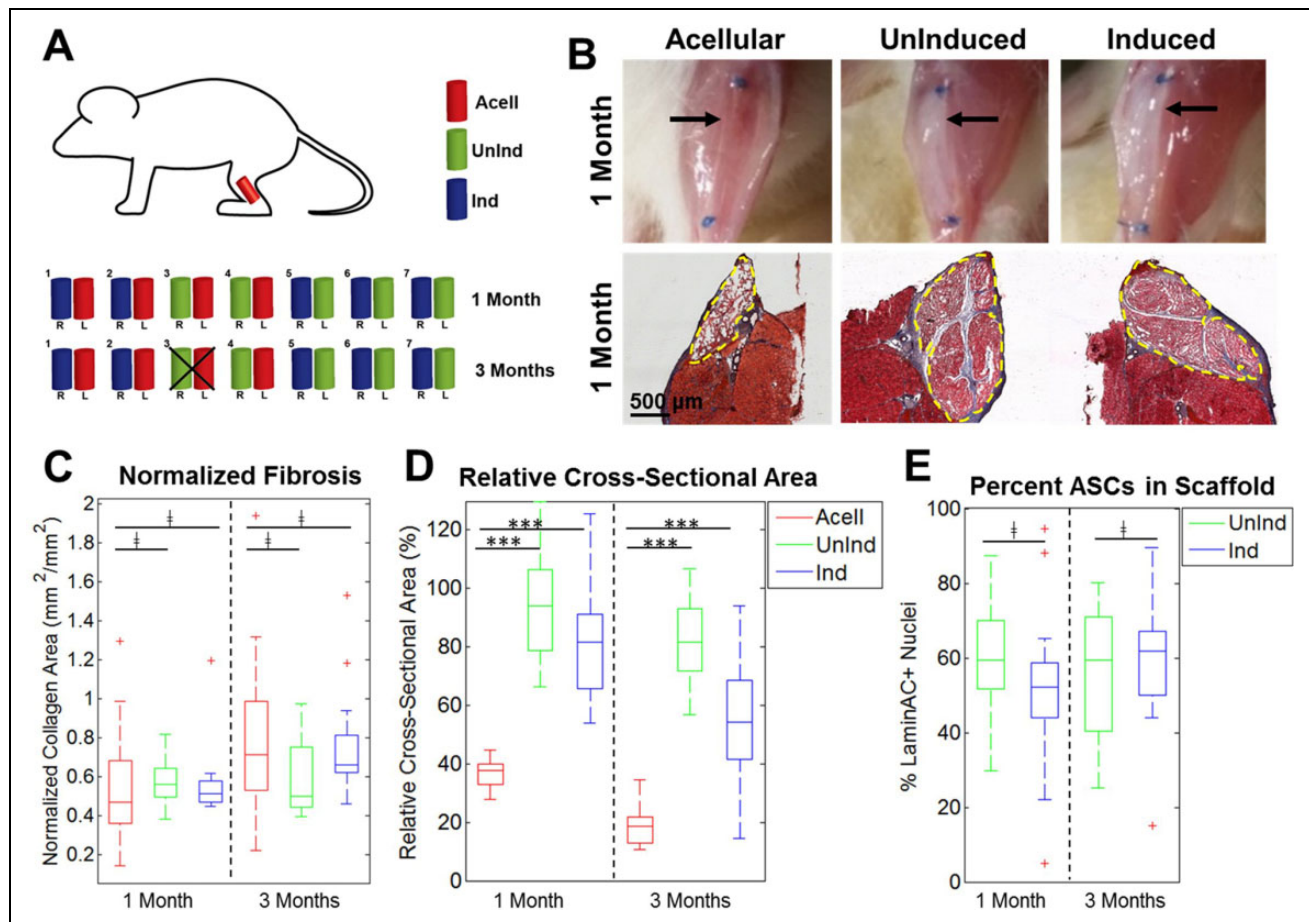


Fig 3. Analysis of cell-seeded fibers implanted in VML defects. (A) Schematic illustrating the experimental plan. Two fibers were implanted per mouse and harvested at 1 or 3 months. Mouse #3 in the 3-month cohort died before the study ended. (B) Differences in appearance were visible between acellular and cell-seeded groups immediately before harvest, with acellular groups appearing more translucent and cell-seeded groups more opaque (top). Black arrows illustrate fiber location within defect site. Masson's Trichrome stain demonstrates minimal fibrosis in all three groups and the larger cross-sectional area present in cell-seeded groups (bottom). Dashed yellow lines denote fiber boundaries. (C) Quantification of normalized fibrosis among all three groups at both time points showed that there were no significant differences between both cell-seeded groups and acellular fibers ($n=9-15$). (D) Quantification of relative cross-sectional area for all three groups at both time points showed that cell-seeded samples had significantly higher retention of cross-sectional area than acellular samples ($n=9-15$). (E) Quantification of the percent of LaminAC+ nuclei in both cell-seeded groups showed high percentages of ASCs in the harvested scaffolds with no significant difference between groups ($n=12-15$).

*** $p < 0.001$. †not significant.

yields and proliferation rates, and reported myogenic potential^{27,28,41-43,29-31,34,37-40}. Their biological relevance arises from the fact that adipocytes and myoblasts share a common Myf5+ precursor⁵⁰ and brown preadipocytes express high levels of myogenic genes⁵¹. Even so, the ability of ASCs to directly differentiate into myoblasts is limited²⁴. In addition to their differentiation capabilities, ASCs have the potential to promote muscle regeneration by providing a pro-regenerative environment and modulating the immune system^{35,36}. ASCs have also been shown to be pro-angiogenic and the ASC secretome includes the angiogenic factors VEGF, HGF, and IGF-1⁵². The current study assessed the *in vitro* and *in vivo* myogenic potential of both uninduced and induced ASCs on a myomimetic electrospun fibrin scaffold.

The scaffold utilized in this study is highly suited for muscle regeneration and has successfully treated VML when combined with C2C12 myoblasts²⁶. Fibrin is a naturally occurring biocompatible and biodegradable material generated during the blood clotting process. As a scaffold material, it can be degraded gradually *in vivo* in the presence of plasmin. It is a vital component of the native coagulation cascade and thus is present in the native wound healing environment. As a surgical adhesive, *in situ* gelled fibrin hydrogel has been widely used in the clinic with an excellent safety profile⁵³. Electrospinning fibrinogen onto a rotating collection dish where it rapidly crosslinks with thrombin under tension enables internal alignment capture of the hydrogel fiber²¹ that mimics the alignment of fibers in native muscle. Cellular alignment is a prerequisite for the uniaxial

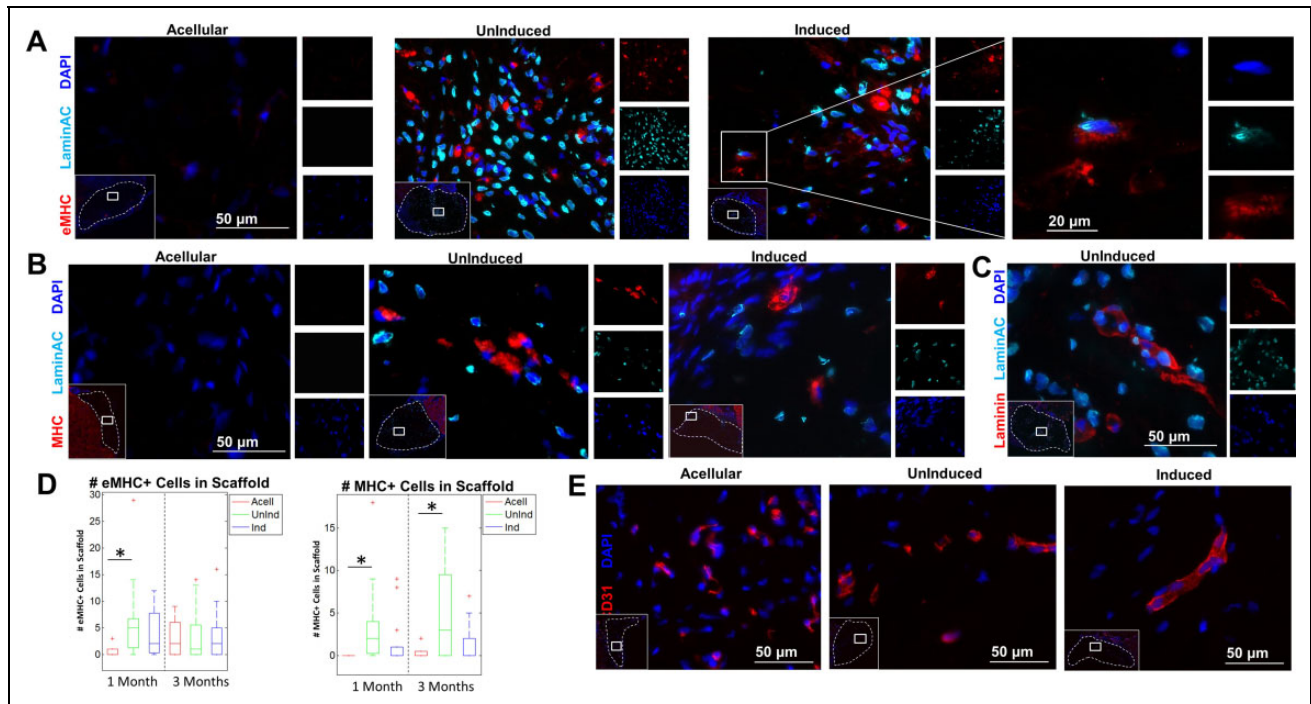


Fig 4. Immunostaining of embryonic myosin, myosin heavy chain, and LaminAC+ nuclei in the fiber interior. (A) Sections of the excised defect site were stained with embryonic myosin (eMHC; red), human-specific LaminAC (cyan), and DAPI (blue). Inset (left): concentrations of eMHC were found in the center of the implanted fibers. Dotted line denotes fiber boundary. Inset (right): Example of colocalizing eMHC+ and human LaminAC+ cell in fibers with induced ASCs. Images depict fibers at 4 weeks. (B) Sections of the excised defect site were stained with myosin heavy chain (MHC; red), human-specific LaminAC (cyan), and DAPI (blue). Inset: concentrations of MHC were found in the center of the implanted fibers. Dotted line denotes fiber boundary. Images depict fibers at 12 weeks. (C) Sections of the excised defect site were stained with laminin (red), human-specific LaminAC (cyan), and DAPI (blue). Inset: concentrations of laminin+ cells with human nuclei were found in the center of the implanted fibers. Dotted line denotes fiber boundary. Image depicts uninduced fibers at 4 weeks. (D) Quantification of the number of eMHC+ and MHC+ cells inside fibers among the three groups ($n=9-15$). There were significantly more eMHC+ cells at 1 month in fibers with uninduced ASCs than in acellular fibers. There was no significant difference in eMHC expression among groups at 3 months. There were significantly more MHC+ cells at both 1 month and 3 months in fibers with uninduced ASCs than in acellular fibers. (E) Sections of the excised defect site were stained for mouse CD31 (red) and DAPI (blue). Inset: host vascular infiltration was found in the interior of the implanted fibers in all groups at 3 months. Dotted line denotes fiber boundary.

* $p < 0.05$.

contraction of functional muscle and construct alignment has been shown to enhance myoblast fusion and stem cell myogenesis^{22,23}. The electrospun fibers also mimic the macroscopic structure of muscle, where groups of muscle fibers are bundled to form fascicles, which in turn are bundled to form the muscle tissue. Each fibrin fiber is a collection of bundled microfibrils, mimicking the native fascicle, and assembling multiple fibrin fibers is scalable to replace an entire muscle. Substrates that mirror the stiffness of native muscle have been shown to enhance stem cell differentiation and myogenesis^{24,25,54}, with an ideal range of 8–17 kPa⁵⁴. The stiffness of the fibrin fibers has been optimized to mimic the mechanics of native muscle with an average Young's Modulus of ~ 17 kPa. In addition to providing an environment that mimics the alignment, structure, and mechanics of native muscle, the electrospun fibrin fibers are suturable and mechanically robust. The fibrin fibers also have the potential to be used as an off-the-shelf material that can be stored long term and rehydrated prior to cell seeding and implantation.

These capabilities, as well as their ability to closely mimic the native muscle environment, make electrospun fibrin fibers a highly suitable candidate material for TE skeletal muscle.

When ASCs were seeded onto the electrospun fibrin fibers, they proliferated to cover the fiber surface and grow into the interior with good cell viability at a range of time points. The fiber surface topography encouraged ASC alignment with the fiber's major axis. Alignment alone has been shown to stimulate increased ASC myogenic differentiation²². To further promote ASC myogenesis, 5-azacytidine was added to the culture medium as a biochemical induction factor. Azacytidine, a DNA methyltransferase inhibitor, has been used previously to encourage both ASC as well as MSC myogenic differentiation by reversing gene silencing and potentially activating a subset of myogenic genes⁵⁵. However, the yield of ASC myogenesis *in vitro* is reported to be as low as 0.1% with potential increases in ASC differentiation when they are co-cultured with myoblasts⁵⁶. This is in

keeping with the *in vitro* components of this study, where ASCs on electrospun fibers attained very low levels of myogenic characteristics after 2 months of culture with no visible differences between uninduced and induced ASCs. It is possible that the fiber alignment^{22,23} and stiffness^{24,25,54} alone may be sufficient to promote the low levels of ASC myogenesis seen, which was not further improved by biochemical induction with 5-azacytidine. ASCs from two donors were used to demonstrate that results are not dependent on age or demographic.

ASCs have much higher reported levels of muscle differentiation when implanted into a regenerating muscle environment *in vivo* than *in vitro* and have demonstrated incorporation into the regenerating muscle tissue⁵⁶. Bacou et al. found that cells from the stromal vascular fraction contributed up to 10% of regenerating muscle fibers in damaged TA muscles⁵⁷, and Di Rocco et al. found that ASCs injected into ischemia-injured adductor muscles contributed up to 10–20% of regenerating fibers²⁸. A number of studies have assessed the muscle regenerative potential of ASCs injected *in vivo*²⁸, but implanting ASCs on a 3D scaffold to assess resulting skeletal muscle formation is still relatively unexplored. ASCs attached to PLGA microsphere carriers transplanted subcutaneously in nude mice formed new muscle tissue after 60 days⁴⁰, and NG2+ ASCs seeded onto hyaluronic acid scaffolds transplanted subcutaneously in nude mice expressed muscle markers after 30 days⁴⁴. Animal models of VML vary greatly in the extent and mechanism of injury, muscle group, and location. VML models previously utilized for TE skeletal muscle include removal of 30% of the TA¹, 50% of the latissimus dorsi⁵⁸, and 75% of the quadriceps muscles³. Regeneration in partial excision models likely relies in part on muscle stem/progenitor cell and vascular ingrowth from the remaining muscle tissue, as it has been shown that muscle progenitor cells can migrate to regenerate distal injuries⁵⁹. Here, we provide a significantly more challenging VML model by excising the entire TA and EDL muscles and utilize this model to assess the muscle regenerative potential of ASCs. The robust VML model used in this study mimics some of the most severe patient cases with little hope for positive regenerative outcomes².

In the current study, ASC-seeded fibers implanted in a VML defect had increased volume retention relative to acellular fibers with uninduced ASCs at 3 months exhibiting up to 4× higher volume retention than acellular fibers. Volume retention for fibers with induced ASCs was slightly lower, but the values for the two cell-seeded groups were not statistically different. This indicates that the addition of ASCs to the fibers preserves them from degradation. Both uninduced and induced ASCs showed low levels of fibrosis, similar ratios of human to mouse cells within the fibers at 3 months post-transplantation, and similar numbers of cells at 3 months that were eMHC+. However, fibers seeded with uninduced ASCs had significantly more regenerating muscle cells positive for MHC when compared with acellular fibers, while fibers seeded with induced ASCs did not. Paired with

the *in vitro* data, this suggests that 5-azacytidine may not be sufficiently potent to induce ASCs down a myogenic lineage, and future studies should evaluate additional biological and biochemical factors that could work synergistically with the biophysical cues provided by the electrospun fibrin fibers.

Despite low levels of muscle regeneration in all treatment groups and limited evidence of ASC myogenesis both *in vitro* and *in vivo*, there is some evidence that ASCs may improve regenerative outcomes for VML. In this study, acellular fibers had eMHC+ regenerating muscle cells at 3 months but no mature MHC+ muscle cells at either time point. Interestingly, ASC-seeded fibers had eMHC expression at 1 month and significantly earlier than that seen in acellular fibers, suggesting that the addition of ASCs hastened the muscle's regenerative response. In addition, unlike the acellular fibers, muscle cells within ASC-seeded fibers were MHC+ at both time points demonstrating the presence of mature muscle cells within the fiber interior. The source of regenerating muscle cells within the fibers is unclear. There were some cases where individual regenerating eMHC+ muscle cells contained Lamin AC+ nuclei but the majority of eMHC+ and MHC+ cells within the fibers did not have an ASC-derived nucleus. In addition, there were laminin+ cells with Lamin AC+ nuclei present in both induced and uninduced ASC samples. It is possible that implanted ASCs directly differentiated into muscle *in vivo* and/or fused with infiltrating host muscle cells. It is important to note that the eMHC, MHC, and laminin antibodies used stain both mouse and human proteins. It is also possible that implanted ASCs provided paracrine signaling to promote muscle progenitor cell infiltration from the host and subsequent regeneration. ASCs are known to provide a pro-regenerative environment and modulate the immune system^{35,36} as well as secrete pro-angiogenic factors⁵². A large number of regenerating muscle cells within the fibers were immediately adjacent to ASCs, suggesting a correlation between ASC location and the presence of regenerating muscle. Our findings suggest that human ASCs promote moderate muscle reconstruction in VML models. Nonetheless, complete removal of the TA and EDL muscles is an aggressive VML injury model for testing the efficacy of this approach due to the lack of endogenous cell infiltration and potential paracrine signaling benefit. It is likely that ASCs implanted in a VML defect involving partial removal of a single muscle would yield further improved regenerative outcomes. Further studies into ASC-mediated muscle regeneration in VML models will be required to understand the mechanism by which ASCs promote regeneration within the harsh VML injury environment.

Conclusions

In this study, the muscle regenerative potential of ASCs combined with an electrospun fibrin fiber mimicking the structure, alignment, and mechanical properties of native

skeletal muscle was assessed. The fibers promoted limited *in vitro* myogenic properties in both induced and uninduced ASCs but both groups failed to fully replicate myotube characteristics *in vitro*. When implanted in a severe VML defect model, the fibers integrated well with the native tissue, eliciting little scarring, promoting long-term survival of transplanted ASCs, and stimulating cellular and vascular ingrowth. Although the number of eMHC+ and MHC+ cells in this model is modest up to 3 months, it should be noted that any amount of muscle regeneration is significant due to the severe VML model that was utilized. Interestingly, *ex vivo* differentiation of ASCs down the myogenic lineage via 5-azacytidine induction did not significantly improve *in vivo* muscle regeneration as was hypothesized. Implanted fibers with uninduced ASCs contained more muscle cells than acellular fibers at both 1 and 3 months, indicating that the addition of uninduced ASCs on electrospun fibrin fibers may enhance muscle regeneration post-VML. In addition, several regenerating muscle cells had LaminAC+ nuclei, indicating the possibility of direct contribution of ASCs to those regenerating cells. Taken together, this data illustrates that despite low *in vitro* myogenic potential, electrospun fibrin fibers combined with ASCs promote moderate muscle reconstruction in a severe VML injury.

Acknowledgements

The authors would also like to thank Justin Morrissette-McAlmon for his help with flow cytometry analysis. This project was funded by partial grant support from the Maryland Stem Cell Research Fund (2016-MSCRFI-2692; MSCRFI-0774) and the NSF (CBET 1350554; DMR1410240). The authors would also like to thank The Wilmer Imaging and Microscopy Core Grant (P30-EY001765) for use of the Zeiss LSM 510 confocal.

Author Contributions

J. Gilbert-Honick conceived and performed experiments and wrote the manuscript.

B. Ginn developed the microfiber bundles and electrospinning process. Y. Zhang performed all animal surgeries. S. Salehi assisted with sample analysis and data acquisition. K. Wagner, H.Q. Mao, and W.L. Grayson conceived experiments, provided expertise in experimental planning and feedback, and edited the manuscript.

Ethical Approval

This study was approved by our institutional review board and institutional animal care and use committee.

Statement of Human and Animal Rights

Biological material was obtained from patients with informed consent and IRB approval. Animal care and surgical procedures were approved by the institutional animal care and use committee at Johns Hopkins University School of Medicine.

Statement of Informed Consent

Biological material was obtained from patients with informed consent and with IRB approval.


Declaration of Conflicting Interests

The authors declared no potential conflicts of interest with respect to the research, authorship, and/or publication of this article.

Funding

The authors received no financial support for the research, authorship, and/or publication of this article.

ORCID iD

Warren L. Grayson  <http://orcid.org/0000-0001-6099-6469>

Supplemental Material

Supplemental material for this article is available online

References

- Garg K, Ward CL, Hurtgen BJ, Wilken JM, Stinner DJ, Wenke JC, Owens JG, Corona BT. Volumetric muscle loss: persistent functional deficits beyond frank loss of tissue. *J Orthop Res*. 2015;33(1):40–46.
- Grogan BF, Hsu JR. Volumetric muscle loss. *J Am Acad Orthop Surg*. 2011;19(suppl 1):S35–S37.
- Sicari BM, Rubin JP, Dearth CL, Wolf MT, Ambrosio F, Boninger M, Turner NJ, Weber DJ, Simpson TW, Wyse A, Brown EH, Dziki JL, Fisher LE, Brown S, Badylak SF. An acellular biologic scaffold promotes skeletal muscle formation in mice and humans with volumetric muscle loss. *Sci Transl Med*. 2014;6(234):234ra58.
- Quarta M, Cromie M, Chacon R, Blonigan J, Garcia V, Akiemenko I, Hamer M, Paine P, Stok M, Shrager JB, Rando TA. Bioengineered constructs combined with exercise enhance stem cell-mediated treatment of volumetric muscle loss. *Nat Commun*. 2017;8:15613.
- Conconi MT, De Coppi P, Bellini S, Zara G, Sabatti M, Marzaro M, Franco Zanon G, Gamba PG, Parnigotto PP, Nussdorfer GG. Homologous muscle acellular matrix seeded with autologous myoblasts as a tissue-engineering approach to abdominal wall-defect repair. *Biomaterials*. 2005;26(15):2567–2574.
- Corona BT, Ward CL, Baker HB, Walters TJ, Christ GJ. Implantation of *in vitro* tissue engineered muscle repair constructs and bladder acellular matrices partially restore *in vivo* skeletal muscle function in a rat model of volumetric muscle loss injury. *Tissue Eng Part A*. 2014;20(3–4):705–715.
- Aurora A, Roe JL, Corona BT, Walters TJ. An acellular biologic scaffold does not regenerate appreciable *de novo* muscle tissue in rat models of volumetric muscle loss injury. *Biomaterials*. 2015;67:393–407.
- Corona BT, Wu X, Ward CL, McDaniel JS, Rathbone CR, Walters TJ. The promotion of a functional fibrosis in skeletal muscle with volumetric muscle loss injury following the transplantation of muscle-ECM. *Biomaterials*. 2013;34(13):3324–3335.
- Dziki J, Badylak S, Yabroudi M, Sicari B, Ambrosio F, Stearns K, Turner N, Wyse A, Boninger ML, Brown EHP, Rubin JP. An acellular biologic scaffold treatment for volumetric muscle

- loss: results of a 13-patient cohort study. *NPJ Regen Med.* 2016;1:16008.
10. Mase VJ, Hsu JR, Wolf SE, Wenke JC, Baer DG, Owens J, Badylak SF, Walters TJ. Clinical application of an acellular biologic scaffold for surgical repair of a large, traumatic quadriceps femoris muscle defect. *Orthopedics.* 2010;33(7):511.
 11. Ma J, Holden K, Zhu J, Pan H, Li Y. The application of three-dimensional collagen-scaffolds seeded with myoblasts to repair skeletal muscle defects. *J Biomed Biotechnol.* 2011; 2011:812135.
 12. Rossi CA, Flaibani M, Blaauw B, Pozzobon M, Figallo E, Reggiani C, Vitiello L, Elvassore N, De Coppi P. In vivo tissue engineering of functional skeletal muscle by freshly isolated satellite cells embedded in a photopolymerizable hydrogel. *FASEB J.* 2011;25(7):2296–2304.
 13. Grasman JM, Do DM, Page RL, Pins GD. Rapid release of growth factors regenerates force output in volumetric muscle loss injuries. *Biomaterials.* 2015;72:49–60.
 14. Kim JH, Ko IK, Atala A, Yoo JJ. Progressive muscle cell delivery as a solution for volumetric muscle defect repair. *Sci Rep.* 2016;6(1):38754.
 15. Page RL, Malcuit C, Vilner L, Vojtic I, Shaw S, Hedblom E, Hu J, Pins GD, Rolle MW, Dominko T. Restoration of skeletal muscle defects with adult human cells delivered on fibrin microthreads. *Tissue Eng Part A.* 2011;17(21–22):2629–2640.
 16. Passipieri JA, Baker HB, Siriwardane M, Ellenburg M, Vad-havkar M, Saul JM, Tomblyn S, Burnett L, Christ GJ. Keratin hydrogel enhances in vivo skeletal muscle function in a rat model of volumetric muscle loss. *Tissue Eng Part A.* 2017; 23(11–12):556–571.
 17. Baker HB, Passipieri JA, Siriwardane M, Ellenburg M, Vad-havkar M, Bergman CR, Saul JM, Tomblyn S, Burnett L, Christ GJ. Cell and growth factor loaded keratin hydrogels for treatment of volumetric muscle loss (VML) in a mouse model. *Tissue Eng Part A.* 2017;00:1–13.
 18. Hagiwara K, Chen G, Kawazoe N, Tabata Y, Komuro H. Promotion of muscle regeneration by myoblast transplantation combined with the controlled and sustained release of bFGFcp. *J Tissue Eng Regen Med.* 2016;10(4):325–333.
 19. Ju YM, Atala A, Yoo JJ, Lee SJ. In situ regeneration of skeletal muscle tissue through host cell recruitment. *Acta Biomater.* 2014;10(10):4332–4339.
 20. Shandalov Y, Egozi D, Koffler J, Dado-Rosenfeld D, Ben-Shimol D, Freiman A, Shor E, Kabala A, Levenberg S. An engineered muscle flap for reconstruction of large soft tissue defects. *Proc Natl Acad Sci U S A.* 2014;111(16):6010–6015.
 21. Zhang S, Liu X, Barreto-Ortiz SF, Yu Y, Ginn BP, DeSantis NA, Hutton DL, Grayson WL, Cui FZ, Korgel BA, Gerecht S, Mao HQ. Creating polymer hydrogel microfibrils with internal alignment via electrical and mechanical stretching. *Biomaterials.* 2014;35(10):3243–3251.
 22. Choi YS, Vincent LG, Lee AR, Kretchmer KC, Chirasatitsin S, Dobke MK, Engler AJ. The alignment and fusion assembly of adipose-derived stem cells on mechanically patterned matrices. *Biomaterials.* 2012;33(29):6943–6951.
 23. Chen M, Sun Y, Chen Y. Electrically conductive nanofibers with highly oriented structures and their potential application in skeletal muscle tissue engineering. *Acta Biomater.* 2013;9(3):5562–5572.
 24. Choi YS, Vincent LG, Lee AR, Dobke MK, Engler AJ. Mechanical derivation of functional myotubes from adipose-derived stem cells. *Biomaterials.* 2012;33(8):2482–2491.
 25. Engler AJ, Griffin MA, Sen S, Bönnemann CG, Sweeney HL, Discher DE. Myotubes differentiate optimally on substrates with tissue-like stiffness: pathological implications for soft or stiff microenvironments. *J Cell Biol.* 2004;166(6):877–887.
 26. Gilbert-Honick J, Iyer SR, Somers SM, Lovering RM, Wagner K, Mao H, Grayson W. Engineering functional and histological regeneration of vascularized skeletal muscle. *Biomaterials.* 2018;164:70–79.
 27. de la Garza-Rodea AS, van der Velde-van Dijke I, Boersma H, Goncalves MAFV, van Bekkum DW, de Vries AAF, Knaan-Shanzer S. Myogenic properties of human mesenchymal stem cells derived from three different sources. *Cell Transplant.* 2012;21(1):153–173.
 28. Di Rocco G, Iachininoto MG, Tritarelli A, Straino S, Zacheo A, Germani A, Crea F, Capogrossi MC. Myogenic potential of adipose-tissue-derived cells. *J Cell Sci.* 2006;119(14): 2945–2952.
 29. Mizuno H, Zuk PA, Ph D, Zhu M, Lorenz HP, Benhaim P, Hedrick MH. Experimental Myogenic differentiation by human processed lipoaspirate cells. *Plastic Reconstruct Surg.* 2002;109(1):199–209.
 30. Labusca L, Zugun-Eloae F, Nacu V, Mashayekhi K. Adipose derived stem cells for musculoskeletal regeneration: recent patents and future perspectives. *Recent Patents Regenerat Med.* 2013;3:132–147.
 31. Zhang Y, Zhu Y, Li Y, Cao J, Zhang H, Chen M, Wang L, Zhang C. Long-term engraftment of myogenic progenitors from adipose-derived stem cells and muscle regeneration in dystrophic mice. *Hum Mol Genet.* 2015;24(21):6029–6040.
 32. VanDusen KW, Syverud BC, Williams ML, Lee JD, Larkin LM. Engineered skeletal muscle units for repair of volumetric muscle loss in the tibialis anterior muscle of a rat. *Tissue Eng Part A.* 2014;20(21–22):2920–2930.
 33. Fuoco C, Salvatori ML, Biondo A, Shapira-Schweitzer K, Santoleri S, Antonini S, Bernardini S, Tedesco FS, Cannata S, Seliktar D, Cossu G, Gargioli C. Injectable polyethylene glycol-fibrinogen hydrogel adjuvant improves survival and differentiation of transplanted mesoangioblasts in acute and chronic skeletal-muscle degeneration. *Skeletal Muscle.* 2012; 2(1):24.
 34. Zuk PA, Ph D, Zhu MIN, Mizuno H, Benhaim P, Lorenz HP. Multilineage cells from human adipose tissue: implications for cell-based therapies. *Tissue Eng.* 2001;7(2): 211–228.
 35. Zuk P. Adipose-derived stem cells in tissue regeneration: a review. *ISRN Stem Cell.* 2013;2013(1):1–35.
 36. DelaRosa O, Sánchez-Correa B, Morgado S, Ramírez C, del Río B, Menta R, Lombardo E, Tarazona R, Casado JG. Human adipose-derived stem cells impair natural killer cell function

- and exhibit low susceptibility to natural killer-mediated lysis. *Stem Cells Dev.* 2012;21(8):1333–1343.
37. Bayati V, Sadeghi Y, Shokrgozar MA, Haghighipour N, Azadmanesh K, Amanzadeh A, Azari S. The evaluation of cyclic uniaxial strain on myogenic differentiation of adipose-derived stem cells. *Tissue Cell.* 2011;43(6):359–366.
 38. Gimble JM, Grayson W, Guilak F, Lopez M, Vunjak-Novakovic G. Adipose tissue as a stem cell source for musculo-skeletal regeneration. *Front Biosci (Schol Ed).* 2013;3(225):69–81.
 39. Liu Y, Yan X, Sun Z, Chen B, Han Q, Li J, Zhao RC. Flk-1⁺ Adipose-Derived Mesenchymal Stem Cells Differentiate into Skeletal Muscle Satellite Cells and Ameliorate Muscular Dystrophy in MDX Mice. *Stem Cells Dev.* 2007;16(5):695–706.
 40. Kim M, Choi YS, Yang SH, Hong HN, Cho SW, Cha SM, Pak JH, Kim CW, Kwon SW, Park CJ. Muscle regeneration by adipose tissue-derived adult stem cells attached to injectable PLGA spheres. *Biochem Biophys Res Commun.* 2006;348(2):386–392.
 41. Lee JH, Kemp DM. Human adipose-derived stem cells display myogenic potential and perturbed function in hypoxic conditions. *Biochem Biophys Res Commun.* 2006;341(3):882–888.
 42. Lin Y, Liu L, Li Z, Qiao J, Wu L, Tang W, Zheng X, Chen X, Yan Z, Tian W. Pluripotency potential of human adipose-derived stem cells marked with exogenous green fluorescent protein. *Mol Cell Biochem.* 2006;291(1–2):1–10.
 43. Meligy FY, Shigemura K, Behnsawy HM, Fujisawa M, Kawabata M, Shirakawa T. The efficiency of in vitro isolation and myogenic differentiation of MSCs derived from adipose connective tissue, bone marrow, and skeletal muscle tissue. *In Vitro Cell Dev Biol Anim.* 2012;48(4):203–215.
 44. Desiderio V, De Francesco F, Schiraldi C, De Rosa A, La Gatta A, Paino F, d'Aquino R, Ferraro GA, Tirino V, Papaccio G. Human Ng2⁺ adipose stem cells loaded in vivo on a new crosslinked hyaluronic acid-lys scaffold fabricate a skeletal muscle tissue. *J Cell Physiol.* 2013;228(8):1762–1773.
 45. Pilia M, McDaniel JS, Guda T, Chen XK, Rhoads RP, Allen RE, Corona BT, Rathbone CR. Transplantation and perfusion of microvascular fragments in a rodent model of volumetric muscle loss injury. *Eur Cell Mater.* 2014;28(210):11–24.
 46. Kesireddy V. Evaluation of adipose-derived stem cells for tissue-engineered muscle repair construct-mediated repair of a murine model of volumetric muscle loss injury. *Int J Nanomedicine.* 2016;11:1461–1473.
 47. Dubois SG, Floyd EZ, Zvonic S, Kilroy G, Wu X, Carling S, Halvorsen YDC, Ravussin E, Gimble JM. Isolation of Human Adipose-derived Stem Cells from Biopsies and Liposuction Specimens. *Methods Mol Biol.* 2008;449:69–79.
 48. Yilgor Huri P, Cook CA, Hutton DL, Goh BC, Gimble JM, DiGirolamo DJ, Grayson WL. Biophysical cues enhance myogenesis of human adipose derived stem/stromal cells. *Biochem Biophys Res Commun.* 2013;438(1):180–185.
 49. Zhang Y, King OD, Rahimov F, Jones TI, Ward CW, Kerr JP, Liu N, Emerson CP Jr, Kunkel LM, Partridge TA, Wagner KR. Human skeletal muscle xenograft as a new preclinical model for muscle disorders. *Hum Mol Genet.* 2014;23(12):3180–3188.
 50. Rosenwald M, Wolfrum C. The origin and definition of brite versus white and classical brown adipocytes. *Adipocyte.* 2014;3(1):4–9.
 51. Timmons JA, Wennmalm K, Larsson O, Walden TB, Lassmann T, Petrovic N, Hamilton DL, Gimeno RE, Wahlestedt C, Baar K, Nedergaard J, Cannon B. Myogenic gene expression signature establishes that brown and white adipocytes originate from distinct cell lineages. *Proc Natl Acad Sci U S A.* 2007;104(11):4401–4406.
 52. Salgado AJ, Reis RL, Sousa NJ, Gimble JM. Adipose tissue derived stem cells secretome: soluble factors and their roles in regenerative medicine. *Curr Stem Cell Res Ther.* 2010;5(2):103–110.
 53. Mandell SP, Gibran NS. Fibrin sealants: surgical hemostat, sealant and adhesive. *Expert Opin Biol Ther.* 2014;14(6):821–830.
 54. Engler AJ, Sen S, Sweeney HL, Discher DE. Matrix elasticity directs stem cell lineage specification. *Cell.* 2006;126(4):677–689.
 55. Rosca AM, Burlacu A. Effect of 5-azacytidine: evidence for alteration of the multipotent ability of mesenchymal stem cells. *Stem Cells Dev.* 2011;20(7):1213–1221.
 56. Dechesne Claude, F. Pisani Didier, Goudenege Sébastien, Dani Christian. Adipose-Derived Stem Cells and Skeletal Muscle Repair. 2011;77–87.
 57. Micallef J, Bacou F, Boubaker R, Levin JM, Chammas M, Casteilla L, Reyne Y, Nougue J. Transplantation of adipose tissue-derived stromal cells increases mass. *Cell Transplant.* 2004;13(33):103–111.
 58. Machingal MA, Corona BT, Walters TJ, Kesireddy V, Koval CN, Dannahower A, Zhao W, Yoo JJ, Christ GJ. A tissue-engineered muscle repair construct for functional restoration of an irrecoverable muscle injury in a murine model. *Tissue Eng Part A.* 2011;17(17–18):2291–2303.
 59. Watt DJ, Morgan JE, Clifford MA, Partridge TA. The movement of muscle precursor cells between adjacent regenerating muscles in the mouse. *Anatomy Embryol.* 1987;175(4):527–536.